THE JOURNAL OF PHYSICAL CHEMISTRY A

Feature Article

pubs.acs.org/JPCA

Time-Resolved Vibrational Spectroscopy of [FeFe]-Hydrogenase Model Compounds

Jamie L. Bingaman,[†] Casey L. Kohnhorst,[†] Glenn A. Van Meter,[†] Brent A. McElroy,[†] Elizabeth A. Rakowski,[†] Benjamin W. Caplins,[†] Tiffany A. Gutowski,[†] Christopher J. Stromberg,*[,†] Charles Edwin Webster,[§] and Edwin J. Heilweil*[,‡]

[†]Department of Chemistry and Physics, Hood College, 401 Rosemont Avenue, Frederick, Maryland 21701-8524, United States

[‡]Radiation and Biomolecular Physics Division, Physical Measurement Laboratory, National Institute of Standards and Technology, 100 Bureau Drive, Gaithersburg, Maryland 20899-8443, United States

[§]Department of Chemistry, The University of Memphis, 213 Smith Chemistry Building, Memphis, Tennessee 38152-3550, United States

Supporting Information

ABSTRACT: Model compounds have been found to structurally mimic the catalytic hydrogen-producing active site of Fe−Fe hydrogenases and are being explored as functional models. The time-dependent behavior of $Fe_2(\mu\text{-}S_2C_3H_6)(CO)_6$ and $Fe_2(\mu\text{-}S_2C_2H_4)(CO)_6$ is reviewed and new ultrafast UV- and visible-excitation/IR-probe measurements of the carbonyl stretching region are presented. Ground-state and excited-state electronic and vibrational properties of $Fe_2(\mu\text{-}S_2C_3H_6)(CO)_6$ were studied with density functional theory (DFT) calculations. For $Fe_2(\mu\text{-}S_2C_3H_6)(CO)_6$ excited with 266 nm, long-lived signals (τ = 3.7 ± 0.26 μs) are assigned to loss of a CO ligand. For 355 and 532 nm excitation, short-lived (τ = 150 ± 17 ps) bands are observed in addition to CO-loss product. Short-lived transient absorption intensities are smaller for 355 nm and much larger for 532 nm excitation and are assigned to a short-lived photoproduct resulting from excited electronic state structural reorganization of the Fe−Fe bond. Because these molecules are tethered by bridging disulfur ligands, this extended di-iron bond relaxes during the excited state decay. Interestingly, and perhaps fortuitously, the time-dependent DFT-optimized exited-state geometry of $Fe_2(\mu\text{-}S_2C_3H_6)(CO)_6$ with a semibridging CO is reminiscent of the geometry of the Fe_2S_2 subcluster of the active site observed in Fe−Fe hydrogenase X-ray crystal structures. We suggest these wavelength-dependent excitation dynamics could significantly alter potential mechanisms for light-driven catalysis.

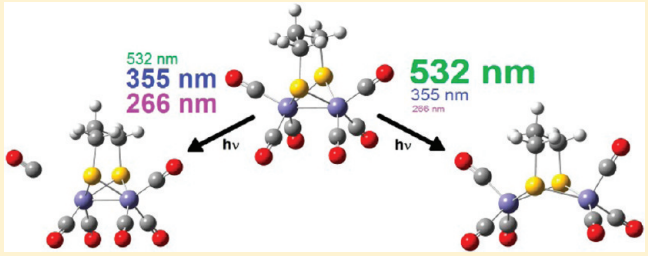

INTRODUCTION

With the main sources of hydrocarbon-based energy currently being depleted, there is a popular interest in the conversion to a hydrogen economy.[1] However, for this shift to actually occur, a cost-effective, efficient, and renewable source of hydrogen fuel is essential. There exist three types of hydrogenases in nature shown to catalyze the reduction of protons to hydrogen gas or the oxidation of hydrogen gas to protons.[2−4] The two most common types are the [NiFe]- and the [FeFe]-hydrogenases. The [NiFe]-hydrogenases, which contain both nickel and iron in the active site, typically catalyze the oxidation of hydrogen to protons, and the [FeFe]-hydrogenases, containing two iron atoms in the active site (Figure 1a), generally catalyze the reduction of protons to molecular hydrogen.[3−9]

In the past few years, studies have been completed on [FeFe]-hydrogenases to enhance the understanding of their structure and function. Attempts have been made to isolate the natural hydrogenases and reproduce their natural catalytic activity. Research involving the immobilization of an [FeFe]-hydrogenase on a TiO_2 electrode proved to be successful with a catalytic efficiency of 70%.[10] The active site of an [FeFe]-hydrogenase has been isolated and its catalytic activity in water was characterized, showing that the active site could potentially be efficient in hydrogen production without the surrounding enzyme.[11] The structure of the active site of [FeFe]-hydrogenase has been refined using computational methods and infrared spectroscopy, revealing the most likely structural candidates for the reduced and oxidized forms of the species.[12]

Recently, there have been many attempts at finding complexes that are structurally related to the hydrogenases in the hopes that these models will have efficient molecular hydrogen producing capabilities similar to the natural [FeFe]-hydrogenase.[13−39] Many of the synthetic compounds contain the same butterfly structure as the hydrogenase, as well as similar ligands and bridge components, and their structures have been characterized using various methods. There has also been research directed toward

Received: December 16, 2011
Revised: May 1, 2012
Published: May 21, 2012

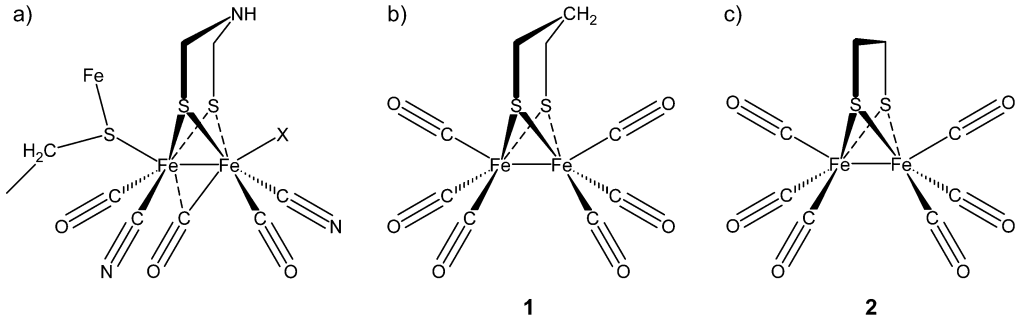

Figure 1. Structure of (a) the active di-iron catalytic center of the native hydrogenase and model species,[3−9] (b) $Fe_2(\mu\text{-}S_2C_3H_6)(CO)_6$ (**1**), and (c) $Fe_2(\mu\text{-}S_2C_2H_4)(CO)_6$ (**2**) studied in this work.

investigating the catalytic activity of various models of [FeFe]-hydrogenase and how different structural characteristics affect the degree of catalytic activity.[40−48]

One specific family of synthetic di-iron compounds that has been found to structurally mimic the active site structure of the natural [FeFe]-hydrogenases contains an iron−iron bond, a disulfur bridge connecting the two iron atoms, and six pendent ligands, such as cyanos, carbonyls, and phosphines.[2−4] Many of these compounds are based on the compounds $Fe_2(\mu\text{-}S_2C_3H_6)(CO)_6$, **1** (Figure 1b), and $Fe_2(\mu\text{-}S_2C_2H_4)(CO)_6$, **2** (Figure 1c). These model compounds are the subject of great interest because they could potentially act as functional models of the hydrogenases and serve as catalysts in their own right. However, the natural hydrogenases catalyze hydrogen production on the scale of tens of thousands to hundreds of thousands of turnovers per second per molecule, whereas the model compounds are not as efficient, generally exhibiting only tens or hundreds of turnovers per second per molecule.[49]

Previous research included pairing these model compounds with a chromophore that can absorb UV or visible light to drive the production of hydrogen, using a mechanism similar to Photosynthesis II.[50] Understanding the detailed time-dependent behavior of these compounds after excitation with UV or visible light is fundamental to determining their suitability for this type of mechanism.

Model compound **1** has previously been studied in detail by the Hunt group using ultrafast UV-excitation, IR-probe[51,52] and UV-excitation 2D-IR probe[48] methods but only using one excitation wavelength (350 nm). However, previous research on similar di-iron compounds indicates that their behavior upon ultrafast laser excitation strongly depends on the wavelength of excitation,[53−57] which is addressed by work reported here.

This Feature Article reports new time-resolved infrared spectral measurements of **1** and **2** using several UV and visible excitation wavelengths, as well as ground state and excited state electronic and vibrational properties of **1** from the results of density functional theory calculations. The ultrafast spectral dynamics of these compounds are compared to previous similar investigations and provide information regarding structural changes that occur in the molecule over picosecond to microsecond time scales. These studies result in a better understanding of the products of these model compounds when excited with UV or visible light. This provides information that could be of importance if these model compounds are considered for hydrogen-producing mechanisms involving light-driven catalysis.

EXPERIMENTAL AND COMPUTATIONAL METHODS[58]

Syntheses. Synthesis of **1** was conducted according to literature methods.[2] The $Fe_3(CO)_{12}$ and 1,3-propanedithiol (purchased from Sigma-Aldrich and used as received) were combined in a nitrogen atmosphere, heated to 350 K, and allowed to react for 3−5 h. After the reaction completed, the sample was filtered and evaporated to dryness under vacuum. It was then washed with hexanes and evaporated to dryness again. Synthesis of **2** was carried out in a similar fashion, but $Fe_3(CO)_{12}$ was combined with 1,2-ethanedithiol.

Time-Resolved UV−Visible Excitation/IR Probe Laser Spectroscopy (TRIR). A Nd:vanadate diode-pumped laser (10 ps, 2 W output at 532 nm, 80 MHz) was used to synchronously pump two tunable dye lasers and seed a 20 Hz Nd:YAG regenerative amplifier.[53] The two dye lasers, one tuned to 656 nm and the other to 589 nm, were amplified by the 25 mJ/pulse, 532 nm output of the Nd:YAG regenerative amplifier and combined to produce 150 fs tunable broad-band IR pulses (ca. 80 cm^{-1} full width at half-maximum) ranging from 1930 to 2100 cm^{-1}. For short-delay experiments (0 to 750 ps), the residual of the Nd:YAG amplifier was also used to generate optically delayed 50−70 ps excitation pulses at 266, 355, and 532 nm. For long-delay experiments (10 ns to 15 μs), a separate, electronically timed Nd:YAG laser (~5 ns pulse width) was used to generate 532, 355, and 266 nm excitation pulses. Typical excitation pulse energies were between 50 and 150 microjoules per pulse at the sample (corresponding to 266 and 532 nm) and the pump and probe beam sizes were approximately 0.5 mm and 0.1 mm diameter, respectively. The estimated maximum peak pump fluence corresponds to at most 1.2 GW/cm^2 at the sample.

The excitation and probe beams were combined and focused into solutions of **1** and **2** in argon-purged *n*-heptane. Typical solution concentrations were chosen so the optical densities (OD) for both pump and probe static absorption feature wavelengths were less than OD = 1 when flowed through a 2 mm path length cell fitted with CaF_2 windows. Half of the generated IR probe beam was sent through a separate part of the solution to provide a spectral reference signal. The IR signal and reference beams were sent through a monochromator and onto a 256 × 256 pixel InSb focal plane detector for spectral analysis (ca. 4 cm^{-1} fwhm spectral resolution). Averages of 4000−6000 laser shots were acquired to produce transient difference spectra at specified excitation-probe time delays. Under all excitation wavelengths and pulse durations, measured difference spectral intensities were found to be linear with excitation pulse fluence at a given delay time.

dx.doi.org/10.1021/jp2121774 | J. Phys. Chem. A 2012, 116, 7261−7271

Computational Details. Theoretical calculations on **1** and **2** have been carried out using the Gaussian 03W[59] implementation of the BP86[60−62] density functional theory (DFT)[63] using default grids, default convergence criteria, and the TZVP basis sets for all atoms (**BS1**).[64,65] The starting structure for the geometry optimization of compound **1** was from the crystallographic data (Cambridge Crystallographic Data Centre #127014).[66] The effect of altering the Fe−Fe bond distance was determined using a series of structure optimization and IR frequency calculations where the Fe−Fe bond was lengthened by 0.25 Å intervals and held fixed, whereas the remaining structure was allowed to optimize. Similar calculations were also run on **2**.

Further theoretical calculations were performed on **1** using the Gaussian09[67] implementation of B3LYP (the B3 exchange functional[68] and LYP correlation functional)[69] and BVP86[60−62,70−72] using the default pruned fine grids for energies (75, 302), default pruned coarse grids for gradients and Hessians (35, 110) (neither grid is pruned for iron), and nondefault SCF convergence for geometry optimizations (10^{-6}). Excited states were geometry optimized using analytical gradients[73,74] with time-dependent density functional theory (TDDFT).[75] The first three excited states were searched, using between 30 and 50 states solved iteratively. For TDDFT optimizations, the default convergence criteria for the energy (10^{-6}) and wave function (10^{-8}) were used. **BS2**: The basis set for iron (341,341,41) → [3s3p2d] was the Hay and Wadt basis set (BS) and effective core potential (ECP) combination (LanL2DZ)[76] as modified by Couty and Hall, where the two outermost p functions have been replaced by a (41) split of the optimized iron 4p function.[77] The 6-31G(d) basis set[78−80] was used for sulfur atoms, and the 6-31G(d′) basis sets[79,80] were used for all other atoms. All structures were fully optimized (except for the set of Fe−Fe constrained models), analytical frequency calculations were performed on all ground state DFT structures, and numerical frequency calculations were performed on selected TDDFT excited state structures. B3LYP results were deemed less reliable and are not discussed further in the article (see Supporting Information for further details). The simulated spectra in Figure 4 were produced with an in-house program using Gaussian broadening and a bandwidth of 1 cm^{-1}.

RESULTS AND DISCUSSION

TRIR of 1. The TRIR spectra of **1** are shown in Figure 2 from 1930 to 2100 cm^{-1} for different UV and visible-excitation wavelengths at various times after excitation. The ground state complex **1** in *n*-hexane solution at room temperature has five major absorptions in the infrared region at 1981, 1991, 2005, 2035, and 2075 cm^{-1}, as shown in Figure 2d. In the time-resolved differential spectra, these absorptions corresponding to the original molecule **1** are recognized as bleaching features (negative OD), implying that some of the original compound has been lost after excitation. These bleach features are generally expected to extend below the baseline but in some instances do not. This effect is due, in part, to highly intense transient absorptions that result in broad bands that overlap and partially obscure the bleaches. Similar differential mid-infrared absorption spectra have been collected previously of **1** over picosecond to nanosecond time delays using only the excitation wavelength of 350 nm.[51,52] Spectra presented in those papers in some cases exhibited very strong below baseline bleaches resulting from loss of the original compound and relatively weak new absorption features. Discrepancies between previously obtained spectra compared to Figure 2b obtained with 355 nm excitation most likely results from differences in the initial concentration of **1** (in previous work,[50,51] the sample had an OD ∼ 0.5 but path length

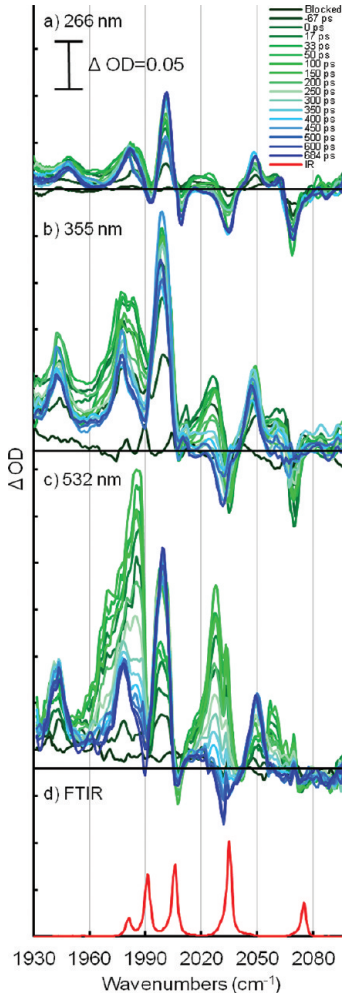

Figure 2. Time-resolved UV or visible excitation, IR probe absorption spectra of **1** in *n*-heptane at 293 K with (a) 266 nm, 70 ps excitation, (b) 355 nm, 70 ps excitation, and (c) 532 nm, 70 ps excitation. (d) IR ground state absorption spectrum of $Fe_2(\mu\text{-}S_2C_3H_6)(CO)_6$ in *n*-hexane for comparison. The IR ground state absorption spectra in hexane and heptane are indistinguishable.

of 100 μm, resulting in a 10-times more concentrated solutions) or the use of much tighter focusing (beam sizes not mentioned) because only 2 μJ per excitation pulse were available. From citations in refs 50 and 51, the excitation beam size of 150 μm and shortest pulse duration employed there (ca. 40 fs) for short-time measurements implies a peak excitation fluence of 220 GW/cm^2, which is more than 2 orders of magnitude higher than for our conditions. Nonlinear effects and spectral distortions from high concentration and tight focusing could lead to the minor spectral differences observed in our respective work using ca. 350 nm excitation (see below).

266 nm Excitation of 1. The time-resolved differential absorption spectra of **1** in *n*-heptane at 293 K using an excitation wavelength of 266 nm are shown in Figure 2a. These data show bleaches from the original molecule, as previously mentioned, as well as a series of long-lived absorptions that persist through 750 ps. Data from longer delay times (not shown) yield a total sample recovery time of 3.7 ± 0.26 μs. This lifetime was extracted from long delay time data for **1** excited at 355 nm. The average of intensities for all the long-lived bands was used because data at other spectral positions did not contain enough time points to obtain a reliable estimate of the decay constant. Previous work

dx.doi.org/10.1021/jp2121774 | J. Phys. Chem. A 2012, 116, 7261−7271

showed evidence of a potential dimerization process at long times (>100 ns), but no evidence of that is seen in our data, probably due to the significantly lower concentration.[51]

In the short-time data, bleach feature peaks are observed at 1991, 2009, 2035, and 2068 cm^{-1} whereas new long-lived absorptions are present at 1950, 1983, 2001, and 2049 cm^{-1}. The slight difference between the four observed bleaches and ground state absorptions is due to small shifts that occur when a bleach signal and a positive absorption signal overlap in TRIR spectroscopy. The time dependence of the absorption bands is presented in Figure 3a. The bleach signals grow to full intensity in about 100 ps (via the excitation pulse integral and shown in Supporting Information) and then decay over the microsecond time scale (not shown). The dynamics of the bleaches after this time delay are difficult to interpret due to their degree of overlap with nearby absorptions.

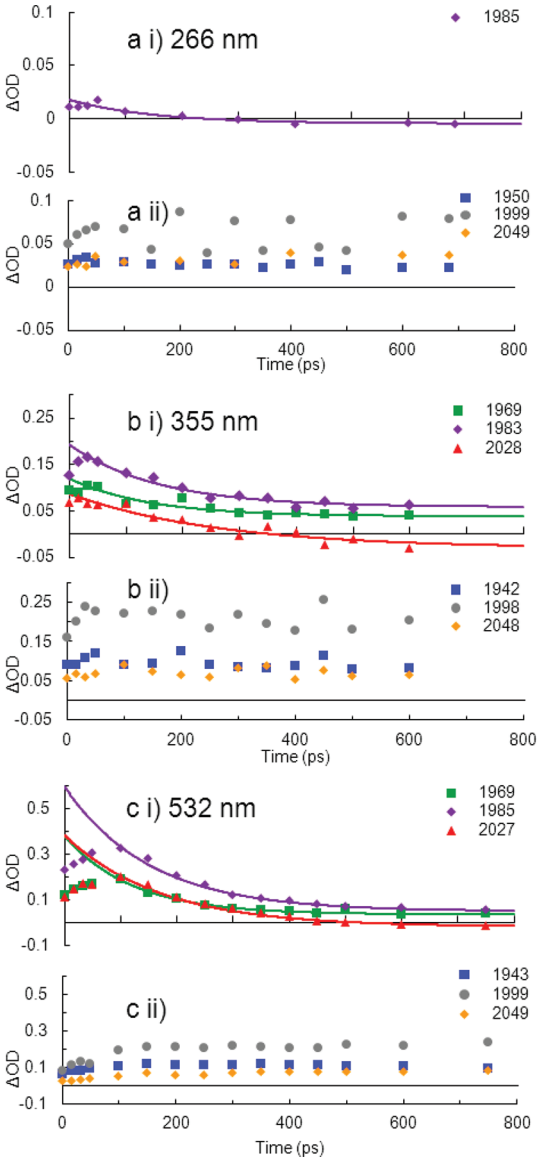

Figure 3. TRIR time dependence for $Fe_2(\mu\text{-}S_2C_3H_6)(CO)_6$ spectral features at selected IR probe wavelengths (cm^{-1}): (a) 266 nm excitation, (b) 355 nm excitation, (c) 532 nm excitation. Short-lived absorptions ($\tau = 150 \pm 17$ ps) are shown with their decaying exponential fits in a-i, b-i, and c-i. Long-lived absorptions ($\tau = 3.7 \pm 0.26$ μs) are shown in a-ii, b-ii, and c-ii. The long-time data used to extract the microsecond time constant are not shown in this figure (see Supporting Information).

The long-lived bands are believed to be evidence of a CO-loss photoproduct, as assigned previously.[48,51,52] These long-lived bands are quite similar to those observed in earlier work; however, the previously observed short-lived absorptions are not present using this excitation wavelength. The observation of microsecond spectral recovery is attributed to bimolecular diffusion-controlled CO recombination with the CO-dissociated molecule, which is expected to occur on the microsecond time scale at the millimolar concentrations used in these experiments.[48,51,52]

355 nm Excitation of 1. The time-resolved differential absorption spectra of **1** in *n*-heptane at 293 K using an excitation wavelength of 355 nm were measured to compare to the previous results[48,51,52] and are shown in Figure 2b. The 355 nm data exhibit long-lived absorptions, which grow in by about 50 ps and are similar in structure and location to those in the 266 nm data, but there are also absorptions present that decay on a much faster time scale. These short-lived absorptions have decayed to stable intensities by 750 ps. After 750 ps, the major change in the spectra is the slow overall (microsecond) recovery to the baseline (data not shown). The bleaches are again present, as they are in the 266 nm excitation data.

In these data, short-lived transient absorption features are discernible near 1969, 1978, 2027, and 2061 cm^{-1}. These short-lived bands reach maximum intensity by about 50 ps, as shown in the time-dependent traces shown in Figure 3b-i, before decaying with a global time constant of 180 ± 46 ps. This behavior is consistent for all of the short-lived bands. The overlap of the short-lived bands with the bleaches makes it difficult to analyze the dynamics of the underlying bleaches. The transient absorptions at 1969 and 1978 cm^{-1} decay to reveal the presence of an underlying long-lived broad absorption feature centered around 1978 cm^{-1}. The time dependence of this long-lived absorption and the others that are comparable to those present in the 266 nm data are displayed in the traces of Figure 3b-ii and again decay back to baseline on the microsecond time scale. These results appear very similar to the results published previously,[48,51,52] with the exception of the difference in relative intensity of the bleaches mentioned earlier.

532 nm Excitation of 1. The time-resolved infrared differential absorption spectra of **1** in *n*-heptane at 293 K with an excitation wavelength of 532 nm are shown in Figure 2c. The 532 nm data display similar structure and features as the 355 nm data, and the absorption feature locations are almost identical for the two excitation wavelengths. The time dependence of the bands in this data is shown in Figure 3c, where the short-lived bands (Figure 3c-i) exhibit a time constant of 150 ± 17 ps and the long-lived bands (Figure 3c-ii) decay with 3.7 ± 0.26 μs time constant. This short-lived decay constant is not significantly different than that measured using the 355 nm excitation data. The 532 nm data have a lower uncertainty than that for the 355 nm excitation of **1** because there is a higher percentage of short-lived absorption bands in the 532 nm data. Thus, the time constant for the 532 nm data is a better measurement of the actual time constant. The major difference between the 532 and 355 nm excitation wavelengths is the relative intensities of the new absorbance bands. The short-lived bands appear with a much higher intensity in the 532 nm data than the 355 nm data.

In previous TRIR work,[48,51,52] the decay of these short-lived bands was assigned to geminate recombination of CO caged within the first solvent shell. This assignment is not supported by

dx.doi.org/10.1021/jp2121774 | J. Phys. Chem. A 2012, 116, 7261–7271

Table 1. Calculated CO-Stretching Frequencies and Intensities for Various Fe−Fe Bond Lengths of 1

2.50 Å[a]		2.75 Å		3.00 Å		3.25 Å		3.50 Å		3.75 Å		4.00 Å	
ω_{harm}[b]	int	ω_{harm}	int	ω_{harm}	int	ω_{harm}	int	ω_{harm}	int	ω_{harm}	int	ω_{harm}	int
1975	306	1973	322	1970	301	1966	271	1960	273	1956	290	1952	274
1983	806	1980	867	1975	951	1970	1019	1965	1052	1961	1071	1956	1135
1983	3	1986	3	1988	3	1987	0	1985	1	1982	21	1979	65
2000	1110	1999	1151	1997	1204	1994	1257	1990	1303	1986	1326	1982	1319
2025	1459	2024	1580	2022	1802	2019	2083	2015	2390	2011	2704	2008	2990
2061	518	2059	506	2057	473	2053	428	2049	382	2045	336	2040	303
total intensity	4202		4429		4734		5059		5402		5748		6085

[a]Bond length from crystal structure. [b]Frequencies are given in wavenumbers.

our new data, however, as the amount of geminate recombination should not radically increase upon visible excitation. If, in fact, geminate recombination did change with the wavelength of excitation, the long-lived signals would be expected to decrease as the short-lived signals increase, due to the lack of CO-dissociated photoproduct after the short-lived time scale has elapsed. Also, the time scale of this decay is not consistent with geminate recombination, as this process would be expected to be significantly faster, usually on the femtosecond to short picosecond time scale for an in-cage mechanism.[81]

Previous studies of $[FeCp(CO)_2]_2$ showed similar wavelength-dependent behavior after excitation.[53−57] In these studies, the photoproduct favored by UV excitation was also attributed to CO loss, and the photoproduct favored by visible excitation was assigned to breaking of the Fe−Fe bond resulting in two radical species. Consequently, what was previously assigned as geminate recombination[48,51,52] may be evidence of a short-lived excited electronic state with a partially elongated Fe−Fe bond. Because the unreactive disulfide bridge constrains the two iron atoms to be in close proximity after electronic excitation and Fe−Fe separation, relatively fast return to the equilibrium bond length and reformation of the Fe−Fe bond could be the source of the decay of the short-lived transient absorbing species.

To test the validity of this possibility, BP86/BS1 DFT calculations were performed on **1** to gradually lengthen the Fe−Fe bond distance of the ground state structure, and the resulting wavenumber shifts and relative intensities of the six major absorptions were calculated (Table 1). The equilibrium bond distance was found to be 2.54 Å from these calculations, which is in agreement with the crystal structure.[66] The BP86 DFT calculations indicate that lengthening of the Fe−Fe bond distance results in higher intensities for most of the CO-stretching absorptions and shifts to lower frequencies, which is observed for separations up to 4.25 Å (at which point the molecular structure breaks apart). The lowest and highest wavenumber absorptions are two exceptions; even though the frequency red shifts as the bond is lengthened, the intensity decreases. The trend for an increase in oscillator strength and shifts to lower frequencies as the Fe−Fe bond is lengthened is consistent with the characteristics of the short-lived absorptions found in the 532 and 355 nm data, supporting the assignment of these features to transient lengthening of the Fe−Fe bond.

Time-dependent excited state BVP86/BS2 DFT calculations were also performed on **1**, and the results indicate that these short-lived absorptions could result from a metal−ligand charge transfer (MLCT) or a metal−metal charge transfer (MMCT) excited singlet state. In these excited states, the metal−metal electron configuration is rearranged, resulting in the two iron atoms acquiring different charges; the molecule then consists of Fe(II) and Fe(0) partial charges instead of the neutral species containing Fe(I) and Fe(I). This difference in charge also results in the lengthening of the Fe−Fe bond with concomitant increase in CO-stretching transition dipole moments. This effect potentially explains the observation of short-lived (with lifetime ca. 100 ps) higher intensity absorptions than observed bleach features. The calculated CO-stretching region spectrum for the MMCT excited state normalized to the ground state frequencies is shown in Figure 4 and can be compared to the 532 nm TRIR experimental spectrum of Figure 2c.

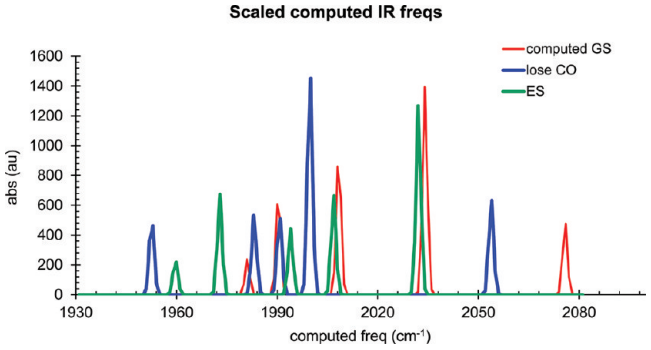

Figure 4. Simulated spectra for the CO-stretching region for **1** from BVP86/BS2 computed frequencies for ground state (red), excited electronic state (green), and CO-loss (blue) species. All spectra were least-squares normalized to the experimental ground state spectral frequencies (see Supporting Information for further details) and may be compared to Figure 2c.

The presence of long-lived CO-loss absorptions in the 532 nm excitation TRIR data was unexpected. Even though previous assignments[48,51,52] and DFT calculations have shown that long-lived pentacarbonyl product bands (at 1943, 1978, 1999, and 2049 cm^{-1}) result from a CO-loss photoproduct, visible-excitation induced photolysis has typically been incapable of causing dissociation of a terminal Fe−CO ligand in similar metal−carbonyls.[82,83] The possibility that these bands are the result of a two-photon process was investigated, and all signals were found to be linear in the excitation energy (see below). When the bond dissociation energy for $Fe(CO)_5$ (2.88×10^{-19} J)[84] is compared to the energy of a 532 nm photon (3.73×10^{-19} J), there is sufficient energy in a 532 nm photon to accomplish Fe−CO photolysis if the energy is confined to the Fe−C coordinate. This analysis suggests that the loss of a CO using visible wavelength excitation is at least plausible. The experimental results indicate that the photoproducts produced via photolysis of **1** are wavelength dependent, as is found for other metal carbonyls, but unlike similar di-iron compounds, **1** undergoes both Fe−Fe bond lengthening, in the excited

dx.doi.org/10.1021/jp2121774 | J. Phys. Chem. A 2012, 116, 7261−7271

electronic state, and Fe−CO cleavage when excited with visible light.

The strength of the short-lived absorption features in the 532 nm TRIR data raised the question as to whether or not they were potentially generated by a two-photon absorption effect. One argument against this notion is that a two-photon absorption for 532 nm excitation would resemble the 266 nm data, and because these two sets of data differ significantly in both relative intensities and transient absorption features, the conclusion can be drawn that the transient signals for the 532 nm data are not a result of two-photon processes. Also, to check for multiphoton absorption effects, the power of the 532 nm excitation pulses was reduced, and both the long-lived and short-lived absorptions reduced proportionately in intensity. Thus, the observed signals are linear in excitation power and do not arise from multiphoton absorption effects.

The dominance of the long-lived bands in the 266 nm data and the presence of the short-lived bands in the 355 and 532 nm data can also be explained from the UV−vis spectra of **1** (green trace in Figure 5). The strong absorptions at 215 and 325 nm

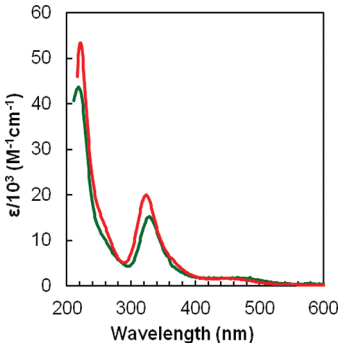

Figure 5. UV−vis absorption spectra of **1** (green trace) and **2** (red trace).

correspond to metal−ligand charge transfer transitions, whereas the relatively weak but broad absorption at 465 nm corresponds to a metal−metal charge transfer transition.[83] Thus, for 266 nm excitation, most of the absorbed energy is directly funneled into dissociation of a carbonyl ligand. However, at 355 nm, there is an apparent overlap of the metal−ligand and metal−metal transitions, causing both carbonyl loss and elongation of the Fe−Fe bond in the excited electronic state. For 532 nm excitation, long-lived bands resulting from carbonyl ligand loss are still observed; however, there is a much higher intensity of the short-lived absorptions because the metal−metal charge transfer transition in the absorption spectrum is centered around 465 nm. CO-loss using 450 nm excitation was not observed in a related disulfur-bridged system,[83] but this was for the compound $Fe_2(CO)_6(\mu\text{-}S_2)$, photolyzed for seconds in a nujol matrix at low temperatures (≪140 K). It is entirely possible that subtle electronic differences between the $Fe_2(CO)_6(\mu\text{-}S_2)$ species and **1** preclude CO-ejection in $Fe_2(CO)_6(\mu\text{-}S_2)$ or that recombination within the solvent cage occurs in the low-temperature matrix on a much more rapid time scale. Because the solvent is a solid at low temperature, the solvent cage is fixed and an ejected CO cannot readily leave the cage and geminate recombination will be much more likely.

TRIR of 2. For comparison to results discussed above for **1**, the time-resolved differential spectra of **2** in *n*-heptane solution from 1930 to 2100 cm^{-1} utilizing the same excitation wavelengths as for **1** are shown in Figure 6. The ground state IR spectrum of this compound is very similar to that of **2**, with

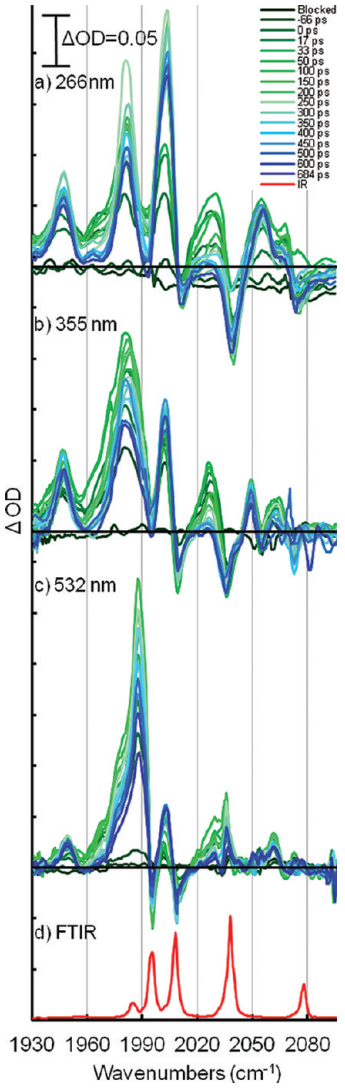

Figure 6. Time-resolved UV and visible excitation, IR probe absorption spectra of **2** in n-heptane with (a) 266 nm, 70 ps excitation, (b) 355 nm, 70 ps excitation, and (c) 532 nm, 70 ps excitation. (d) FT-IR spectrum of $Fe_2(\mu\text{-}S_2C_2H_4)(CO)_6$.

five major ground state CO-stretch absorptions occurring at 1986, 1996, 2008, 2038, and 2078 cm^{-1}, as shown in Figure 6d. These results represent a 4 cm^{-1} shift from the spectrum of **1**, but otherwise the spectra are essentially identical.

266 nm Excitation of 2. The time-resolved differential absorption spectra of **2** in *n*-heptane at 293 K and with 266 nm excitation are shown in Figure 6a. These data exhibit a set of long-lived absorptions present at 1948, 1983, 2004, and 2056 cm^{-1}. These absorptions are shown as the blue traces of Figure 6a. There also exists a broad, relatively short-lived absorption around 2030 cm^{-1}, which seems to be absent in the data for **1**. On the basis of the strength of the band in the 266 nm data (and its relatively lower strength in 355 and 532 nm data), this band may result from vibrational cooling of the molecule.

355 and 532 nm Excitation of 2. The time-resolved spectra of **2** using 355 and 532 nm are shown in Figure 6b,c, respectively. The major long-lived absorptions in these sets of data are found in locations similar to those in Figure 6a, and the time dependence of these features are displayed in Figure 7b-i,c-i, respectively. Compared to the data for **1**, there is less evidence of the short-lived absorptions present in the data for **2**.

dx.doi.org/10.1021/jp2121774 | J. Phys. Chem. A 2012, 116, 7261−7271

Also, whereas the short- versus long-lived band locations in **1** result in two distinct sets of bands, the short- and long-lived bands in **2** have similar frequencies. These observations may be explained by referring to the structure of **2**. When compared to the structure of **1**, complex **2** has one less carbon in its disulfur bridge (Figure 1) and thus possesses less flexibility. This constrained structure would make lengthening the Fe−Fe bond less likely, resulting in reduced intensity for the short-lived bands.

Overall, the observed dynamics for **2** are similar to those of **1**, and a similar excitation wavelength dependence is found. Shorter excitation wavelengths favor CO loss, whereas longer excitation wavelengths favor Fe−Fe bond lengthening, although to a lesser extent in **2** than in **1**.

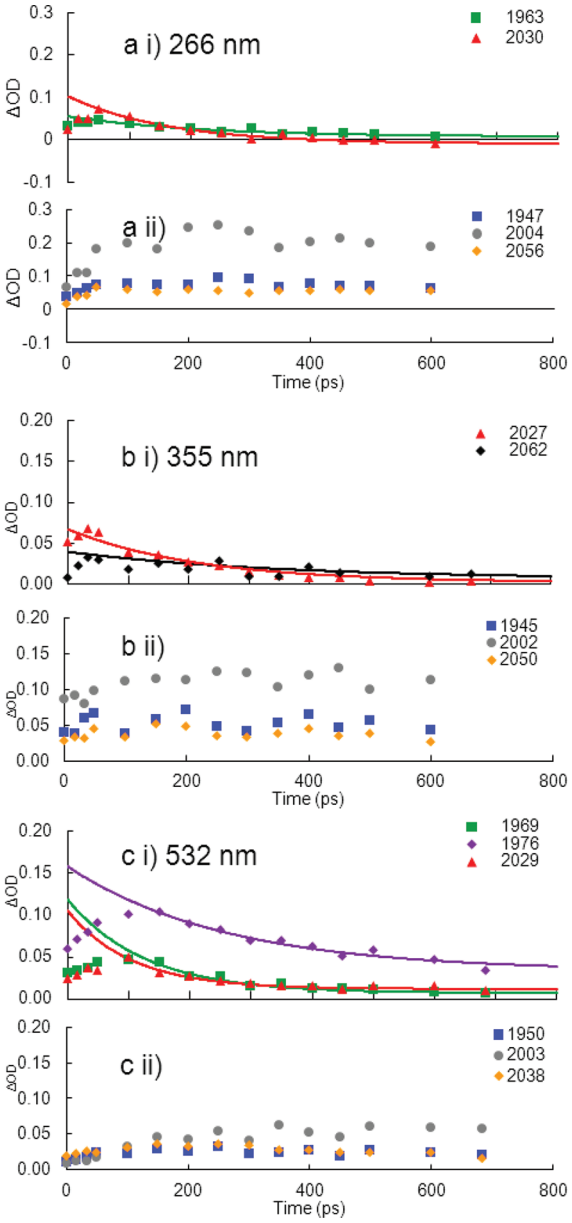

Figure 7. TRIR time dependence for $Fe_2(\mu\text{-}S_2C_2H_4)(CO)_6$ features at selected IR probe wavelengths (cm^{-1}): (a) 266 nm excitation; (b) 355 nm excitation; (c) 532 nm excitation. Short-lived absorptions ($\tau = 190 \pm 62$ ps) are shown with their decaying exponential fits in a -i, b-i, and c-i. Long-lived absorptions ($\tau \approx 3$ μs) are shown without their fits in a-ii, b-ii, and c-ii.

CONCLUSIONS AND FUTURE PROSPECTS

Our ultrafast UV- and visible-excitation/IR-probe experiments revealed that the photochemistry of **1** and **2** are strongly dependent on the wavelength of excitation. UV and visible excitation produces CO-loss and Fe−Fe bond-lengthened intermediates, with visible excitation of **1** producing more excited electronic state population with a lengthened Fe−Fe bond, whereas UV excitation produces relatively more CO-loss photoproduct. Unexpectedly, significant CO loss was observed using 532 nm excitation, a trend not previously seen in similar metal carbonyls (such as $[CpFe(CO)_2]_2$). Given these new findings and interpretations for the short-lived absorptions present in our 532 and 355 nm excitation experiments, transients previously assigned to geminate recombination[48,51,52] are now assigned to a photoproduct that is an excited electronic state with a partially elongated Fe−Fe bond. The functional hydrogenase species is actually deactivated when exposed to CO and reactivated by exposure to UV light. Thus, the presence or absence of CO-ligand loss in this data could indicate whether these compounds catalytically function in a manner similar to that for the native hydrogenase.

In related work by others in recent years, these model compounds have been paired with light-harvesting chromophores in an attempt to achieve catalysis in a mechanism similar to Photosynthesis II.[50] This strategy has generally assumed, however, that the active site of the molecule is unchanged when exposed to the light intended to excite the chromophore. Given the results presented above, a substantial portion of the molecules will undergo structural changes upon exposure to UV or visible light, with some of these changes persisting for microseconds. This dynamic behavior of the active site needs to be accounted for when considering these and related light-driven catalysis mechanisms. Such unreactive dynamical mechanisms may be minimized by selecting a UV sensitive chromophore, rather than one activated only by visible excitation.

Further experiments are planned and underway to investigate the time-resolved spectroscopy of related model hydrogenase compounds of the form $[Fe_2(\mu\text{-}S_2R)(CO)_{6-n}(CN)_n]^{n-}$, where the bridging R group is either propyl or ethyl and n is either 1 or 2. These species are more closely related to the wild-type catalytic center, because they also contain pendant cyano groups attached to the di-iron core. Although the photodissociation of metal carbonyl species in various environments has been studied extensively over many years, much less attention has been directed toward ionic metal cyanides. Only a few recent experiments that focused on vibrational relaxation phenomena and photodynamics of metal-cyanides have been published.[85] These studies involved excitation at available pumping wavelengths (e.g., 800 nm) with visible and mid-infrared probe wavelengths spanning time delays from ca. 5 ps to about 15 μs.

The ionic compounds more closely resemble the actual structure of the active site of the hydrogenase enzyme and provide access to different electronic states at energies that may open up the possibility for other potential photofragments to be generated, including loss of CN from the active site. Investigations of these ionic systems will also be intriguing and more relevant to hydrogen synthesis from protons, because they are soluble in aqueous environments that can be acidified. Although mid-infrared time-resolved probing investigations of hydrogenase mimics in water poses some challenges because water is an extremely strong infrared absorber, related methods employed in TRIR and 2D-IR studies of peptides and proteins (e.g., using ~6 μm flow-cell path length and D_2O as solvent) should be applicable to these systems.[86] On the basis of the results presented in this Feature Article, information regarding the wavelength-dependent photodissociation of these

dx.doi.org/10.1021/jp2121774 | J. Phys. Chem. A 2012, 116, 7261−7271

molecular systems is critical if they are to be considered for pairing with other light-driven catalysts in mechanisms that resemble photosynthesis. The wavelength of light used to fuel synthetic catalysts could, as discussed in this paper, cause significant changes in the structure of the model compounds resulting in their inability to serve in the efficient production of hydrogen.

It has also become very clear that in addition to performing detailed experimental dynamical studies of hydrogenase mimics, confirmation of excited state and structural transient assignments must also be conducted using modern theoretical methods. Application of appropriate DFT functionals and time-dependent techniques to extract potential transient structures, their relative energetics, and time-dependent phenomena will help pave the way toward a fuller understanding of these complex but important systems. We hope the initial time-resolved investigations reviewed and reported in this Feature Article will inspire much more detailed and revealing investigations by other researchers working in hydrogen fuel and related light-driven energy production fields.

■ ASSOCIATED CONTENT

Supporting Information

Further details of computational results, including full citations for refs 59 and 67. Time-dependent decays spanning the picosecond to microsecond time scales for the two model compounds at various representative absorption and bleaching frequencies are also provided. Sample microsecond transient infrared data. This material is available free of charge via the Internet at http://pubs.acs.org.

■ AUTHOR INFORMATION

Corresponding Author

*C.J.S.: e-mail, stromberg@hood.edu; phone, (301) 696-3678; fax, (301) 696-3667. E.J.H.: e-mail, edwin.heilweil@nist.gov; phone, (301) 975-2370; fax, (301) 975-6991.

Notes

The authors declare no competing financial interest.

Biographies

Jamie L. Bingaman graduated with a B.A. in Chemistry and Mathematics from Hood College in May of 2012. She worked under the supervision of Christopher J. Stromberg from Hood and Edwin J. Heilweil from the National Institute of Standards and Technology on research involving time-resolved vibrational spectroscopy of di-iron hydrogenase models as a part of Hood's Summer Research Institute. This paper was also her Departmental Honors Thesis. She will begin graduate work at Pennsylvania State University in the fall of 2012.

Casey L. Kohnhorst worked on the current project as an undergraduate at Hood College (Frederick, MD), where she received her B.A. in Biochemistry in 2010. In 2011 she participated in an internship with Dr. Mehdi Moini at the Smithsonian Institution's Museum Conservation Institute (Suitland, MD), developing new analytical methods to quantitate the age of proteinacious specimens using CE-MS. Casey is now enrolled in the doctoral program at the University of Maryland, Baltimore County, where she works with Dr. Songon An investigating transient multienzyme metabolic complexes (e.g., the Purinosome) using fluorescence microscopy with the aim of better understanding cancer metabolism.

Glenn A. Van Meter graduated from Hood College in 2011 with a bachelor's degree in chemistry. He is employed as a Manufacturing Technician at Lifeline Cell Technology, a biotech company located in Frederick, MD. His current interests pertain to chemical manufacturing and formulation. He hopes to use his research and production experience to help streamline future chemical production practices.

Brent A. McElroy worked on theoretical and physical data collection for iron−iron hydrogenase model compounds during the summer of 2011 at the

National Institute of Standards and Technology. He is currently earning a B.A. with majors in Chemistry and Mathematics at Hood College in Frederick, MD. Previously he has worked in Marine Corps Intelligence, Naval Electronics, and solar cell manufacturing. In the future, Brent wishes to be involved in more research with potential value to alternative energy industries.

Elizabeth A. Rakowski received her B.A in Chemistry from Hood College in 2009. She worked with Christopher Stromberg at Hood College through Hood's Summer Research Institute program. She is currently employed as an Environmental Laboratory Technician for Martel Laboratories in Baltimore, MD, testing samples for organic compounds and metal content.

Benjamin W. Caplins received a B.A. in Chemistry from Hood College in 2009. Under the direction of Christopher J. Stromberg and Edwin J. Heilweil he performed time-resolved vibrational studies of biomimetic metal−carbonyl complexes. He is currently pursuing his Ph.D. at the University of California, Berkeley, under the supervision of Charles B. Harris. His current research uses two-photon photoemission to understand the unique electronic states at metal−organic interfaces.

Tiffany A. Gutowski received her B.A. in Chemistry and Psychology from Hood College in 2009, where she contributed to the featured work under Christopher Stromberg. She is currently employed as an Operations Research Analyst for the U.S. Army Material Systems Analysis Activity and is pursuing a M.A. degree in Chemistry at the University of Delaware.

Christopher J. Stromberg received his B.A. in Chemistry from Gustavus Adolphus College in 1998 and his Ph.D. from Stanford University in 2003, where he worked with Michael D. Fayer studying vibrational dynamics in complex systems using nonlinear ultrafast laser spectroscopy. He completed his postdoctoral work at Pomona College, working with Fred Grieman studying molecular ions using electron impact spectroscopy. He joined the faculty of Hood College in 2005, where he is an Associate Professor and Chair of the Department of Chemistry and Physics. He is currently researching [FeFe]-hydrogenase model compounds using ultrafast laser spectroscopy, as well as using spectroscopy to better understand the structure of gels used in the cleaning of cultural heritage objects.

Photo provided by the University of Memphis.

Charles Edwin Webster received his B.S. in Chemistry and Biochemistry from the University of West Florida in 1995 and his Ph.D. from the University of Florida in 1999, where he worked with Russell S. Drago, Michael C. Zerner, and Michael J. Scott on physical inorganic studies of adsorbate/adsorbent interactions and heterogeneous catalysis. He completed his postdoctoral work at Texas A&M University, working with Michael B. Hall, working on studies of inorganic, bioinorganic, and organometallic catalysis and chemistry. He joined the faculty of the University of Memphis, Department of Chemistry, in 2005, where he is an Associate Professor. His past positions include Assistant Professor, The University of Memphis; Visiting Professor, Zhengzhou University, Department of Chemistry; Research Scientist, Texas A&M University, Department of Chemistry; and Lecturer, Texas A&M University, Department of Chemistry. His current research includes studies of inorganic, bioinorganic, and organometallic chemistry; transition-state

dx.doi.org/10.1021/jp2121774 | J. Phys. Chem. A 2012, 116, 7261−7271

analogues; phosphoryl transfer enzymes; structure and bonding; and homogeneous catalysis.

Edwin J. Heilweil received B.A. degrees in Chemistry and Mathematics and a M.A. degree in Physical Chemistry from Brandeis University (1978). He received his Ph.D. in Physical Chemistry from the University of Pennsylvania under the direction of Robin M. Hochstrasser (1983). From 1984–85 Dr. Heilweil was a NRC Postdoctoral Fellow at NIST (formerly NBS) and is a staff Research Chemist there. During 1986–1991, he developed ultrafast broadband infrared laser methods to examine vibrational energy transfer and photochemical processes of molecules as gases and in liquids and solids. He continues to perform time-resolved vibrational measurements of organometallic photoswitches and Fe–Fe hydrogenase model compounds with academic collaborators. His current research interests include ultrafast far-infrared technologies (Terahertz/THz) and their application to monitor ultrafast chemical reactions, carrier dynamics in conducting polymers and nanolayered structures for solar cells, dynamics of biomolecules in condensed phases, detection of chemical threats and objects in containers for Homeland Security applications.

■ ACKNOWLEDGMENTS

This work was made possible in part through funding to Hood College from the National Institute of Standards and Technology (Cooperative Agreement Numbers 70NANB7H6135 and 70NANBH9125); funding from internal Science, Technical, and Research Support; funding from the National Science Foundation under Grant No. CHE-0911528 (CEW); and computational resources from the University of Memphis High-Performance Computing Facility. Funding was also provided by Hood College's Summer Research Institute through a grant from the Life Technologies Foundation.

■ REFERENCES

(1) Jacoby, M. *Chem. Eng. News Archive* **2003**, *81*, 35.
(2) Gloaguen, F.; Lawrence, J. D.; Schmidt, M.; Wilson, S. R.; Rauchfuss, T. B. *J. Am. Chem. Soc.* **2001**, *123*, 12518.
(3) Wang, X.-B.; Niu, S.; Yang, X.; Ibrahim, S. K.; Pickett, C. J.; Ichiye, T.; Wang, L.-S. *J. Am. Chem. Soc.* **2003**, *125*, 14072.
(4) Popescu, C. V.; Eckard, M. *J. Am. Chem. Soc.* **1999**, *121*, 7877.
(5) Bennett, B.; Lemon, B. J.; Peters, J. W. *Biochemistry* **2000**, *39*, 7455.
(6) Adams, M. W.; Stiefel, E. L. *Chem. Biol.* **2000**, *4*, 214.
(7) Gloaguen, F.; Lawrence, J. D.; Rauchfuss, T. B. *J. Am. Chem. Soc.* **2001**, *123*, 9476.
(8) Nicolet, Y.; Lemon, B. J.; Fontecilla-Camps, J. C.; Peters, J. W. *Trends Biochem. Sci.* **2000**, *25*, 138.
(9) van der Vlugt, J. I.; Rauchfuss, T. B.; Wilson, S. R. *Chem.—Eur. J.* **2006**, *12*, 90.
(10) Morra, S.; Valetti, F.; Sadeghi, S. J.; King, P. W.; Meyer, T.; Gilardi, G. *Chem. Commun.* **2011**, *47*, 10566.
(11) Zipoli, F.; Car, R.; Cohen, M. H.; Selloni, A. *J. Phys. Chem. B* **2009**, *113*, 13096.
(12) Tye, J. W.; Darensbourg, M. Y.; Hall, M. B. *Inorg. Chem.* **2008**, *47*, 2380.
(13) Zhang, Y.; Hu, M.-Q.; Wen, H.-M.; Si, Y.-T.; Ma, C.-B.; Chen, C.-N.; Liu, Q.-T. *J. Organomet. Chem.* **2009**, *694*, 2576.
(14) Erdem, Ö. F.; Schwartz, L.; Stein, M.; Silakov, A.; Kaur-Ghumaan, S.; Huang, P.; Ott, S.; Reijerse, E. J.; Lubitz, W. *Angew. Chem., Int. Ed.* **2011**, *50*, 1439.
(15) de Hatten, X.; Bothe, E.; Merz, K.; Huc, I.; Metzler-Nolte, N. *Eur. J. Inorg. Chem.* **2008**, *2008*, 4530.
(16) Schwartz, L.; Eilers, G.; Eriksson, L.; Gogoll, A.; Lomoth, R.; Ott, S. *Chem. Commun.* **2006**, 520.
(17) Wang, F.; Wang, M.; Liu, X.; Jin, K.; Dong, W.; Sun, L. *Dalton Trans.* **2007**, 3812.
(18) Yu, Z.; Wang, M.; Li, P.; Dong, W.; Wang, F.; Sun, L. *Dalton Trans.* **2008**, 2400.
(19) Li, P.; Wang, M.; Chen, L.; Liu, J.; Zhao, Z.; Sun, L. *Dalton Trans.* **2009**, 1919.
(20) Green, K. N.; Hess, J. L.; Thomas, C. M.; Darensbourg, M. Y. *Dalton Trans.* **2009**, 4344.
(21) Salomone-Stagni, M.; Stellato, F.; Whaley, C. M.; Vogt, S.; Morante, S.; Shima, S.; Rauchfuss, T. B.; Meyer-Klaucke, W. *Dalton Trans.* **2010**, *39*, 3057.
(22) Zhan, C.; Wang, X.; Wei, Z.; Evans, D. J.; Ru, X.; Zeng, X.; Liu, X. *Dalton Trans.* **2010**, *39*, 11255.
(23) Song, L.-C.; Xie, Z.-J.; Liu, X.-F.; Ming, J.-B.; Ge, J.-H.; Zhang, X.-G.; Yan, T.-Y.; Gao, P. *Dalton Trans.* **2011**, *40*, 837.
(24) Durgaprasad, G.; Bolligarla, R.; Das, S. K. *J. Organomet. Chem.* **2011**, *696*, 3097.
(25) Sun, L.; Åkermark, B.; Ott, S. *Coord. Chem. Rev.* **2005**, *249*, 1653.
(26) Petro, B. J.; Vannucci, A. K.; Lockett, L. T.; Mebi, C.; Kottani, R.; Gruhn, N. E.; Nichol, G. S.; Goodyer, P. A. J.; Evans, D. H.; Glass, R. S.; et al. *J. Mol. Struct.* **2008**, *890*, 281.
(27) Czech, I.; Stripp, S.; Sanganas, O.; Leidel, N.; Happe, T.; Haumann, M. *FEBS Lett.* **2011**, *585*, 225.
(28) Chiang, M.-H.; Liu, Y.-C.; Yang, S.-T.; Lee, G.-H. *Inorg. Chem.* **2009**, *48*, 7604.
(29) Wang, N.; Wang, M.; Liu, J.; Jin, K.; Chen, L.; Sun, L. *Inorg. Chem.* **2009**, *48*, 11551.
(30) Singh, P. S.; Rudbeck, H. C.; Huang, P.; Ezzaher, S.; Eriksson, L.; Stein, M.; Ott, S.; Lomoth, R. *Inorg. Chem.* **2009**, *48*, 10883.
(31) Li, B.; Liu, T.; Popescu, C. V.; Bilko, A.; Darensbourg, M. Y. *Inorg. Chem.* **2009**, *48*, 11283.
(32) Keita, B.; Floquet, S.; Lemonnier, J.-F.; Cadot, E.; Kachmar, A.; Benard, M.; Rohmer, M.-M.; Nadjo, L. *J. Phys. Chem. C* **2008**, *112*, 1109.
(33) Wang, H.-Y.; Wang, W.-G.; Si, G.; Wang, F.; Tung, C.-H.; Wu, L.-Z. *Langmuir* **2010**, *26*, 9766.
(34) Song, L.-C.; Yang, Z.-Y.; Hua, Y.-J.; Wang, H.-T.; Liu, Y.; Hu, Q.-M. *Organometallics* **2007**, *26*, 2106.
(35) Gao, W.; Song, L.-C.; Yin, B.-S.; Zan, H.-N.; Wang, D.-F.; Song, H.-B. *Organometallics* **2011**, *30*, 4097.
(36) Song, L.-C.; Wang, H.-T.; Ge, J.-H.; Mei, S.-Z.; Gao, J.; Wang, L.-X.; Gai, B.; Zhao, L.-Q.; Yan, J.; Wang, Y.-Z. *Organometallics* **2008**, *27*, 1409.
(37) Song, L.-C.; Zeng, G.-H.; Lou, S.-X.; Zan, H.-N.; Ming, J.-B.; Hu, Q.-M. *Organometallics* **2008**, *27*, 3714.
(38) Harb, M. K.; Niksch, T.; Windhager, J.; Görls, H.; Holze, R.; Lockett, L. T.; Okumura, N.; Evans, D. H.; Glass, R. S.; Lichtenberger, D. L.; et al. *Organometallics* **2009**, *28*, 1039.
(39) Song, L.-C.; Luo, X.; Wang, Y.-Z.; Gai, B.; Hu, Q.-M. *J. Organomet. Chem.* **2009**, *694*, 103.
(40) Harb, M. K.; Apfel, U.-P.; Sakamoto, T.; El-khateeb, M.; Weigand, W. *Eur. J. Inorg. Chem.* **2011**, *2011*, 986.
(41) Aušra, J.; Wright, J. A.; Pickett, C. J. *Eur. J. Inorg. Chem.* **2011**, *2011*, 1033.
(42) Gao, W.; Sun, J.; Åkermark, T.; Li, M.; Eriksson, L.; Sun, L.; Åkermark, B. *Chem.—Eur. J.* **2010**, *16*, 2537.

(43) Harb, M. K.; Windhager, J.; Daraosheh, A.; Görls, H.; Lockett, L. T.; Okumura, N.; Evans, D. H.; Glass, R. S.; Lichtenberger, D. L.; El-khateeb, M.; et al. *Eur. J. Inorg. Chem.* **2009**, *2009*, 3414.
(44) Apfel, U.-P.; Kowol, C. R.; Morera, E.; Görls, H.; Lucente, G.; Keppler, B. K.; Weigand, W. *Eur. J. Inorg. Chem.* **2010**, *2010*, 5079.
(45) Wright, J. A.; Pickett, C. J. *Chem. Commun.* **2009**, 5719.
(46) Kaziannis, S.; Wright, J. A.; Candelaresi, M.; Kania, R.; Greetham, G. M.; Parker, A. W.; Pickett, C. J.; Hunt, N. T. *Phys. Chem. Chem. Phys.* **2011**, *13*, 10295.
(47) Jiang, S.; Liu, J.; Sun, L. *Inorg. Chem. Commun.* **2006**, *9*, 290.
(48) Stewart, A. I.; Wright, J. A.; Greetham, G. M.; Kaziannis, S.; Santabarbara, S.; Towrie, M.; Parker, A. W.; Pickett, C. J.; Hunt, N. T. *Inorg. Chem.* **2010**, *49*, 9563.
(49) Adams, M. W. W.; Stiefel, E. I. *Science* **1998**, *282*, 1842.
(50) Wolpher, H.; Borgstrom, M.; Hammarstrom, L.; Bergquist, J.; Sundstrom, V.; Styring, S.; Sun, L.; Akermark, B. *Inorg. Chem. Commun.* **2003**, *6*, 989.
(51) Kaziannis, S.; Santabarbara, S.; Wright, J. A.; Greetham, G. M.; Towrie, M.; Parker, A. W.; Pickett, C. J.; Hunt, N. T. *J. Phys. Chem. B* **2010**, *114*, 15370.
(52) Ridley, A. R.; Stewart, A. I.; Adamczyk, K.; Ghosh, H. N.; Kerkeni, B. n.; Guo, Z. X.; Nibbering, E. T. J.; Pickett, C. J.; Hunt, N. T. *Inorg. Chem.* **2008**, *47*, 7453.
(53) Dougherty, T. P.; Grubbs, W. T.; Heilweil, E. J. *J. Phys. Chem.* **1994**, *98*, 9396.
(54) George, M. W.; Dougherty, T. P.; Heilweil, E. J. *J. Phys. Chem.* **1996**, *100*, 201.
(55) Anfinrud, P. A.; Han, C. H.; Lian, T.; Hochstrasser, R. M. *J. Phys. Chem.* **1991**, *95*, 574.
(56) Moore, J. N.; Hansen, P. A.; Hochstrasser, R. M. *J. Am. Chem. Soc.* **1989**, *111*, 4563.
(57) Dixon, A. J.; George, M. W.; Hughes, C.; Poliakoff, M.; Turner, J. J. *J. Am. Chem. Soc.* **1992**, *114*, 1719.
(58) Certain commercial equipment, instruments, or materials are identified in this paper to adequately specify the experimental procedure. In no case does identification imply recommendation or endorsement by NIST.
(59) Frisch, M. J.; Trucks, G. W.; Schlegel, H. B.; Scuseria, G. E.; Robb, M. A.; Cheeseman, J. R.; Montgomery, J., J., A.; Vreven, T.; Kudin, K. N.; Burant, J. C.; et al. *Gaussian 03*, Revision E.01; Gaussian, Inc.: Wallingford, CT, 2004.
(60) Becke, A. D. *Phys. Rev. A* **1988**, *38*, 3098.
(61) Perdew, J. P. *Phys. Rev. B* **1986**, *33*, 8822.
(62) Perdew, J. P. *Phys. Rev. B* **1986**, *34*, 7406.
(63) Parr, R. G.; Yang, W. *Density-Functional Theory of Atoms and Molecules*; Oxford University Press: New York, 1989.
(64) Schafer, A.; Horn, H.; Ahlrichs, R. *J. Chem. Phys.* **1992**, *97*, 2571.
(65) Schafer, A.; Huber, C.; Ahlrichs, R. *J. Chem. Phys.* **1994**, *100*, 5829.
(66) Lyon, E. J.; Georgakaki, I. P.; Reibenspies, J. H.; Darensbourg, M. Y. *Angew. Chem., Int. Ed.* **1999**, *38*, 3178.
(67) Frisch, M. J.; Trucks, G. W.; Schlegel, H. B.; Scuseria, G. E.; Robb, M. A.; Cheeseman, J. R.; Scalmani, G.; Barone, V.; Mennucci, B.; Petersson, G. A.; et al. *Gaussian 09*, Revsion A.02; Gaussian Inc.: Wallingford, CT, 2009.
(68) Becke, A. D. *J. Chem. Phys.* **1993**, *98*, 5648.
(69) Lee, C.; Yang, W.; Parr, R. G. *Phys. Rev. B* **1988**, *37*, 785.
(70) Perdew, J. P.; Zunger, A. *Phys. Rev. B* **1981**, *23*, 5048.
(71) Vosko, S. H.; Wilk, L.; Nusair, M. *Can. J. Phys.* **1980**, *58*, 1200.
(72) In Gaussian, when the P86 correlation functional is specified, this keyword combines non-local Perdew correlation with Perdew–Zunger81 local correlation. When the VP86 correlation functional is specified, Gaussian uses VWN5 local correlation instead of Perdew–Zunger81.
(73) Furche, F.; Ahlrichs, R. *J. Chem. Phys.* **2002**, *117*, 7433.
(74) Furche, F.; Ahlrichs, R. *J. Chem. Phys.* **2004**, *121*, 12772.
(75) Marques, M. A. L.; Gross, E. K. U. *Annu. Rev. Phys. Chem.* **2004**, *55*, 427.
(76) Hay, P. J.; Wadt, W. R. *J. Chem. Phys.* **1985**, *82*, 299.
(77) Couty, M.; Hall, M. B. *J. Comput. Chem.* **1996**, *17*, 1359.
(78) The 6-31G(d′) basis set has the explonent for the d polarization function for C, O, and N taken from the 6-311G(d) basis sets, instead of the original arbitrarily assigned value of 0.8 used in the 6-31G(d) basis sets.
(79) Hariharan, P. C.; Pople, J. A. *Theor. Chim. Acta* **1973**, *28*, 213.
(80) Hehre, W. J.; Ditchfield, R.; Pople, J. A. *J. Chem. Phys.* **1972**, *56*, 2257.
(81) Kyu Kim, S.; Pedersen, S.; Zewail, A. H. *Chem. Phys. Lett.* **1995**, *233*, 500.
(82) Moore, B. D.; Simpson, M. B.; Poliakoff, M.; Turner, J. J. *J. Chem. Soc., Chem. Commun.* **1984**, *1984*, 972.
(83) Silaghi-Dumitrescu, I.; Bitterwolf, T. E.; King, R. B. *J. Am. Chem. Soc.* **2006**, *128*, 5342.
(84) Lewis, K. E.; Golden, D. M.; Smith, G. P. *J. Am. Chem. Soc.* **1984**, *106*, 3905.
(85) Weidinger, D.; Brown, D. J.; Owrutsky, J. C. *J. Chem. Phys.* **2011**, *134*, 124510.
(86) Hamm, P.; Zanni, M. *Concepts and Methods of 2D Infrared Spectroscopy*; Cambridge University Press: Cambridge, U.K., 2011.